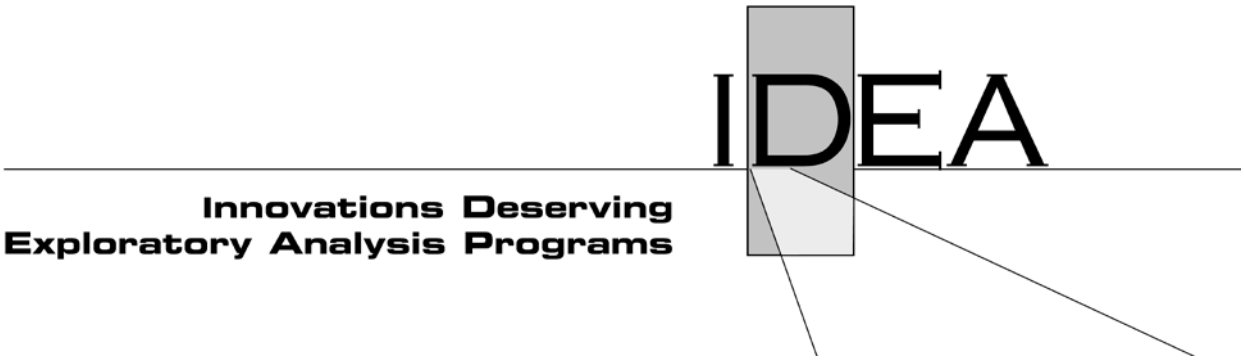

NCHRP IDEA Program

The Stress State Identification of Critical Bridge Components using Nonlinear Acoustics

Final Report for
NCHRP IDEA Project 158

Prepared by:
Didem Ozevin
University of Illinois at Chicago

June 2014

TRB TRANSPORTATION RESEARCH BOARD
The National Academies of
SCIENCES · ENGINEERING · MEDICINE

Innovations Deserving Exploratory Analysis (IDEA) Programs Managed by the Transportation Research Board

This IDEA project was funded by the NCHRP IDEA Program.

The TRB currently manages the following three IDEA programs:

- The NCHRP IDEA Program, which focuses on advances in the design, construction, and maintenance of highway systems, is funded by American Association of State Highway and Transportation Officials (AASHTO) as part of the National Cooperative Highway Research Program (NCHRP).
- The Safety IDEA Program currently focuses on innovative approaches for improving railroad safety or performance. The program is currently funded by the Federal Railroad Administration (FRA). The program was previously jointly funded by the Federal Motor Carrier Safety Administration (FMCSA) and the FRA.
- The Transit IDEA Program, which supports development and testing of innovative concepts and methods for advancing transit practice, is funded by the Federal Transit Administration (FTA) as part of the Transit Cooperative Research Program (TCRP).

Management of the three IDEA programs is coordinated to promote the development and testing of innovative concepts, methods, and technologies.

For information on the IDEA programs, check the IDEA website (www.trb.org/idea). For questions, contact the IDEA programs office by telephone at (202) 334-3310.

IDEA Programs
Transportation Research Board
500 Fifth Street, NW
Washington, DC 20001

The Stress State Identification of Critical Bridge Components using Nonlinear Acoustics

IDEA Program Final Report

Contract Number 158

Prepared for the IDEA Program
Transportation Research Board
The National Academies

Didem Ozevin
University of Illinois at Chicago

June 4, 2014

ACKNOWLEDGEMENT

This investigation was supported by the National Academics, National Academy of Sciences NCHRP IDEA program under Contract No. NCHRP-158 entitled, The Identification of Stress State of Critical Bridge Components using Nonlinear Acoustics. The support from the sponsor is gratefully acknowledged. Any opinions, findings, and conclusions or recommendations expressed in this report are those of the author and do not necessarily reflect the views of the organization acknowledged above. The author would like to thank Illinois DOT and Virginia DOT for providing access to the bridges in Illinois and Virginia, and the technical advisory committee of Professor Jan Achenbach, Dr. Stephen Sharp, Dr. Sepand Momeni, Mrs. Sarah Wilson and Mr. Steve Manstny for the guidance and support provided. The author would like to thank graduate students James Bittner and Zeynab Abbasi for their help throughout the project.

TABLE OF CONTENTS

Executive Summary **4**

IDEA Product **6**

Concept and Innovation **6**

Investigation **7**

Calibration Tests **7**

(1) Uniaxial test 7

(2) Biaxial test – no shear stress 8

(3) Biaxial test – the presence of shear stress 8

Implementation Challenges **9**

(1) The Influence of Paint 9

(2) The Influence of Recoupling Error 11

Field Demonstration **13**

(1) Illinois, Chicago 13

(2) Norris Bridge, Virginia 15

Plans for Implementation **18**

Conclusions **18**

References **19**

EXECUTIVE SUMMARY

This project is developing and demonstrating the application of a nonlinear acoustics-based technique for identifying the stress state of critical highway bridge components through laboratory-scale and field testing. The project involved laboratory-scale and field demonstration of the proposed approach. Theoretical and numerical models were developed to identify the most sensitive ultrasonic waves to the level of stress on structural steel. The selected ultrasonic waves were tested on an L profile loaded uniaxially and a thick plate loaded uniaxially and bi-axially. The load value was increased incrementally, and ultrasonic measurement was taken at each loading step to develop a sensitivity curve of the stress-ultrasonic velocity relationship. Plates with different thicknesses and with and without holes as well as with and without paint were numerically modeled and analyzed under dynamic loading in order to identify variables affecting the ultrasonic waves. The plates were tested under stress-free state for comparing with the numerical results. It was demonstrated both numerically and experimentally that the Rayleigh wave arrival for frequencies above 700 kHz was not influenced by the plate waves for plates thicker than 0.5 inch. A special hand-holder was designed and fabricated that allowed adjusting transmitter-receiver spacing and varying sensor angle to control the propagating waves. The holder keeps the transmitter-receiver distance fixed during stress measurements, preventing any change in distance between the transmitter and the receiver when the structural material is under stress. The effect of bolt holes on the ultrasonic signature was identified. A change in arrival time of 0.03 μsec was identified as the error range to be considered in stress measurement. The structural shapes were tested under uniaxial and biaxial loading to identify the frequency stress calibration curve. The tests were conducted using 1 MHz ultrasonic transducers. The limitations of the approach due to the presence of paint and surface roughness were identified. The peak frequency for a painted sample was 0.66 MHz while that for a similar unpainted sample 0.89 MHz. An approach to overcome the paint influence on the stress-free reference point was developed through taking measurement from low stress region at a gusset plate under investigation in the field. The effect of recoupling on stress measurement was studied and an approach to reduce the coupling error was developed through a surface preparation process. If the coupling fluid was wiped over the testing surface and then wiped smooth, the variation decreased. A laboratory test was performed by placing the sensor wedges parallel to the application of loading. The purpose of this test was to measure the biaxial loading coefficients K_1 (-4.25×10^{-5} MPa^{-1}) and K_2 (4.01×10^{-4} MPa^{-1}) required for complex loading cases.

A fracture critical steel truss bridge provided by the Illinois DOT was modeled using a finite element program. Truss elements were modeled using discrete elements; the gusset plate was modeled as a two-dimensional plate element. The stress levels of the selected points on the gusset plate were identified using numerical simulation. Field measurements, using the hand-held ultrasonic device, the ultrasonic setting, and the correlation curve developed in the laboratory testing, were taken for comparison with the finite element results. To overcome the recoupling error from one measurement point to another, a novel pulse-echo correction method was developed and successfully implemented during field measurements. As the gusset plates are under complex stress state including parallel and perpendicular normal stresses and shear stress, further investigation was performed in the laboratory. It was identified that for a given point, the measurement should be repeated from parallel and perpendicular directions in order to solve two unknown normal stress values. Further laboratory investigation using the data of the recoupled testing device at each load stage indicates that the ultrasonic coupling has significant effect on the measurement. The coupling correction method adjusts the values in logical sequence (i.e., the higher the stress, the lower the ultrasonic frequency). However, it is discovered that if there is a significant presence of shear stress, a third measurement is needed in addition to parallel and perpendicular directions for solving normal and shear stresses. The second bridge testing was performed at Norris Bridge in Virginia, which is a multi-span truss bridge. The measurements from multiple points in gusset plates were taken in two orthogonal directions. The difference between the numerical and experimental results is acceptable considering the complete elastic stress range. Higher error comes from uncertainties in the boundary conditions of the gusset plate model. Currently, the bridge was modeled with sub-structural concept using COMSOL: the gusset plate modeled with shell elements; the connected truss members modeled as simple beam elements. The approach eliminates the assumption of any fixed/free boundary conditions of the gusset plate, which do not represent the actual gusset plate boundary condition.

The summary of the major project outcomes is

(1) The influence of the paint on the reference stress-free measurement leads to selecting the reference point as low stress region on the target gusset plate;
(2) A coupling correction method is developed, which reduces the effect of ultrasonic couplant on the measurement and increases the minimum detectable stress level;
(3) The nonlinearity coefficients in two directions of biaxial loading were quantified for the structural steel in laboratory;
(4) The influence of shear stress is observed due to thickness of gusset plates;

(5) The field measurements have reasonable accuracy under the consideration of measurement uncertainties;
(6) An algorithm of all measurement steps is developed, which can be embedded into the ultrasonic hand-held units for real time assessment of stress at gusset plates.

The tests performed during this project have been able to establish a baseline understanding of stress detection in active structures using ultrasonic surface wave propagation in the frequency domain. During the process many critical factors were uncovered, and initial attempts were made to compensate for each factor. The critical factors experienced were perturbation frequency, surface coupling and unique material zero stress frequency. The approach to each of these areas represents an initial start that allowed a reduction of error to measure viable stress estimations. Each critical factor holds the key to reducing the overall error of the measurement technique. Further blocked research into the application phase of measurement to overcome critical coupling errors is needed. Based on the findings, a methodology to measure stress at gusset plates is developed and shown in FIGURE 1. Additionally during laboratory testing the effect of the shear stress was found to deviate from the theory used in the stress-nonlinearity equation. Further study into the shear effect on surface wave propagation offers an additional area to reduce the overall measurement error.

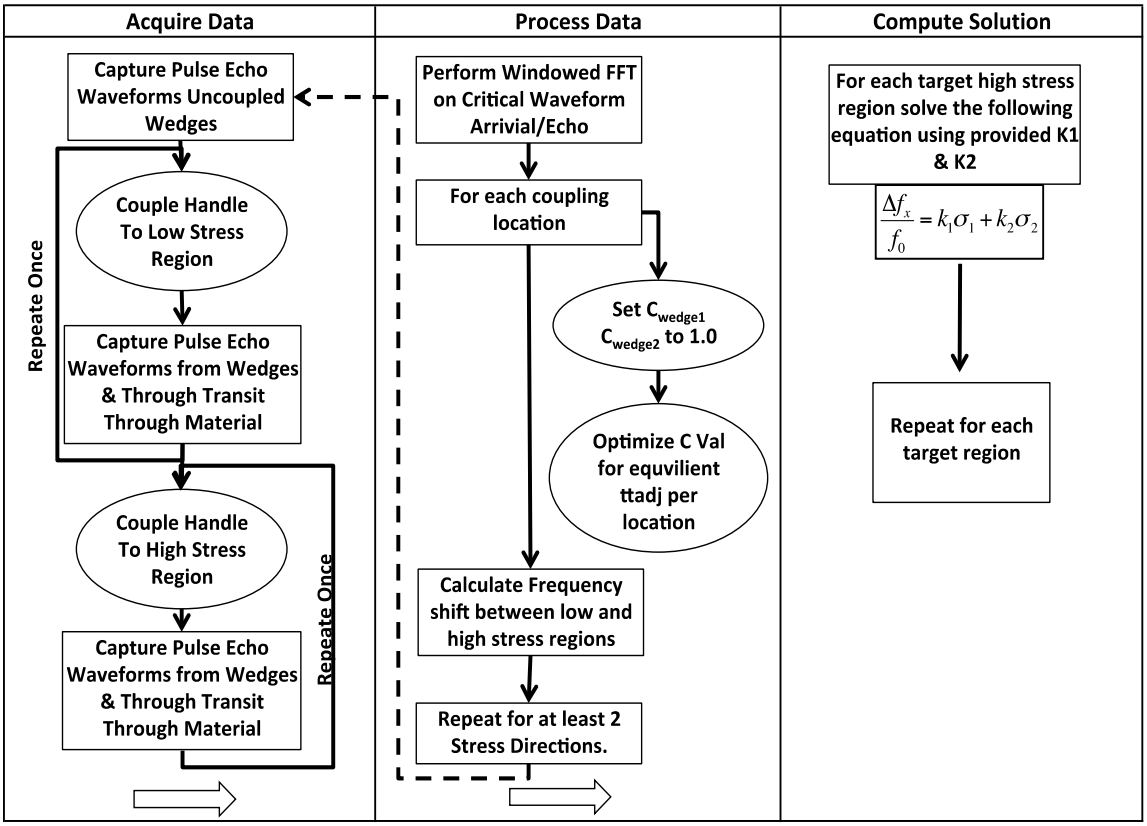

FIGURE 1 The proposed stress measurement methodology for gusset plates.

IDEA PRODUCT

FIGURE 2a and b show the dimensions and picture of the measurement equipment. The hand-held UT equipment is a Pocket UT device manufactured by Mistras Group. This device is a combination of AD-IPR-1210 Digital to Analog Oscilloscope and a 0-400 Volt variable signal generator. The wedges selected for Rayleigh wave generation are variable angle beam wedges constructed by Olympus Inspection & Measurement Systems. The transducers used were Panametrics A401S and were selected from Olympus to match the variable angle beam wedges. The supplied and verified longitudinal wave velocity of the wedge was 2720 m/s. The measured wave velocity of the A572 Grade 50 steel was found via pulse-echo technique to be approximately 5950 m/s. The required second critical angle was calculated to be approximately 62.7^o. The wedges were adjusted to this incident angle and secured for the duration of testing. A handle is constructed to position the wedges apart at a constant distance and surface orientation. The handle was constructed out of plexi-glass to prevent any ultrasonic wave leakage from distorting the Rayleigh arrival.

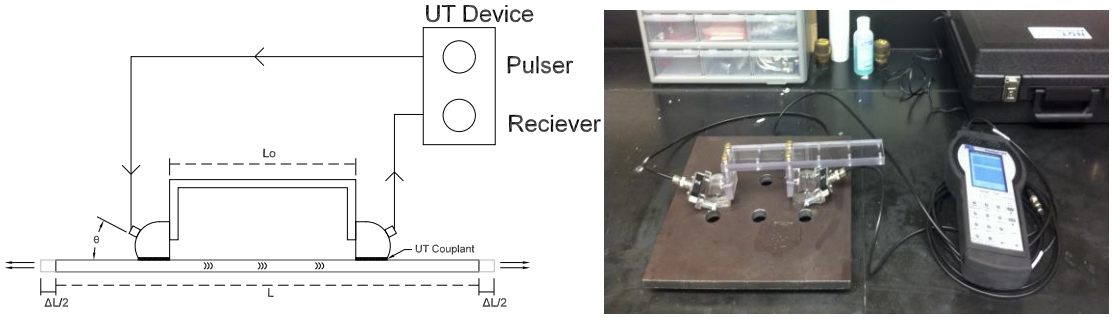

FIGURE 2 Measurement system, (a) design layout, (b) equipment.

CONCEPT AND INNOVATION

In this project, the fundamental challenges of bridge gusset plates such as surface texture, roughness, paint influence, and sensor recoupling are investigated experimentally. Findings indicate each is a critical variable in low stress ranges where the acoustoelastic effect is weak. A method to reduce the recoupling error is proposed. Rayleigh waves at 1 MHz are selected for building the stress-frequency relationships in order to reduce the effect of varying gusset plate thicknesses and surface textures. In order to fix the transmitter-receiver distance for generating Rayleigh waves, special holder is designed, similar to [14, 23], and implemented during the calibration tests and field tests. The acoustoelastic coefficients are identified using uniaxial and biaxial loads on 3/8 inch thick A572 hot rolled steel plates. The proposed algorithm is demonstrated on a recoupled test where the ultrasonic transducers are coupled to the plate after each load increment.

The general method of measurement in this study is to generate a spike 1 MHz perturbation to the stressed structure through a piezoelectric ultrasonic transducer. The wedge is positioned at the second critical angle to initiate Rayleigh surface waves as shown in FIGURE 2a. As the wave propagates into the stressed steel, the wave distortion occurs adjusting the velocity and ultimately the frequency. As the distance between the receiver and the transmitter is fixed, the relationship between arrival time change and stress can be written as:

$$\Delta t = \frac{l_o}{V_o(1+K\sigma)} \tag{1}$$

The arrival time difference Δt is measured in the frequency domain in this study. This eliminates the precise identification of the arrival time in time domain, which can introduce additional errors.

Jassby and Saltoun [8] showed the general equation of the acoustoelastic velocity effect in a biaxial stress solution. Equation 2 provides two material-dependent stress acoustic coefficients K_1 and K_2. Based on the analytical solutions, the shear stress is noted as having no effect on the Rayleigh stress wave propagation.

$$\frac{v-v_o}{v_o} = K_1\sigma_{11} + K_2\sigma_{22} \tag{2}$$

The biaxial loading condition shows that there are two unknowns in a complex loaded material, which are parallel stress σ_{11} and perpendicular stress σ_{22}. Therefore, two measurements need to be taken from a given point on a gusset plate in order to obtain two inputs. The measurement system is oriented in <1> direction to obtain $\langle\frac{\Delta f}{f_0}\rangle_1$ and then rotated 90^o to

obtain $\langle\frac{\Delta f}{f_0}\rangle_2$, where f the peak perturbation arrival frequency. The stresses σ_{11} and σ_{22} can be solved using equations 3 and 4 if the nonlinearity coefficients K_1 and K_2 are known.

$$\langle\frac{\Delta f}{f_0}\rangle_1 = K_1\sigma_{11} + K_2\sigma_{22} \tag{3}$$

$$\langle\frac{\Delta f}{f_0}\rangle_2 = K_1\sigma_{22} + K_2\sigma_{11} \tag{4}$$

INVESTIGATION

CALIBRATION TESTS

(1) Uniaxial test

The first study attempted was to confirm that the resolution of the handheld device was able to detect the weak stress effect on frequency. To observe the stress affect a 3/8-in (9.525mm) A592 steel plate was stressed over a stepped range and a wedge handle introduced a perturbation onto the surface. The testing apparatus and setup configuration are illustrated in FIGURE 3. The perturbation arrival was used to observe the shift in peak frequency, FIGURE 3. At each step a waveform was captured and the Fast Fourier Transform was performed on the Rayleigh wave arrival using the window of 58.97 μs to 61.97 μs time window (corresponds to 300 points of data and two cycles). The peak frequency in the FFT result was recorded and compared against the peak frequency experienced at a zero stress load. This measurement compares only against an unloaded state so any residual stress from rolling is not included. In FIGURE 4b the percent change in peak frequency is plotted against the loaded stress with the nonlinearity coefficient K_1 as -4.1x10^{-5} MPa^{-1}.

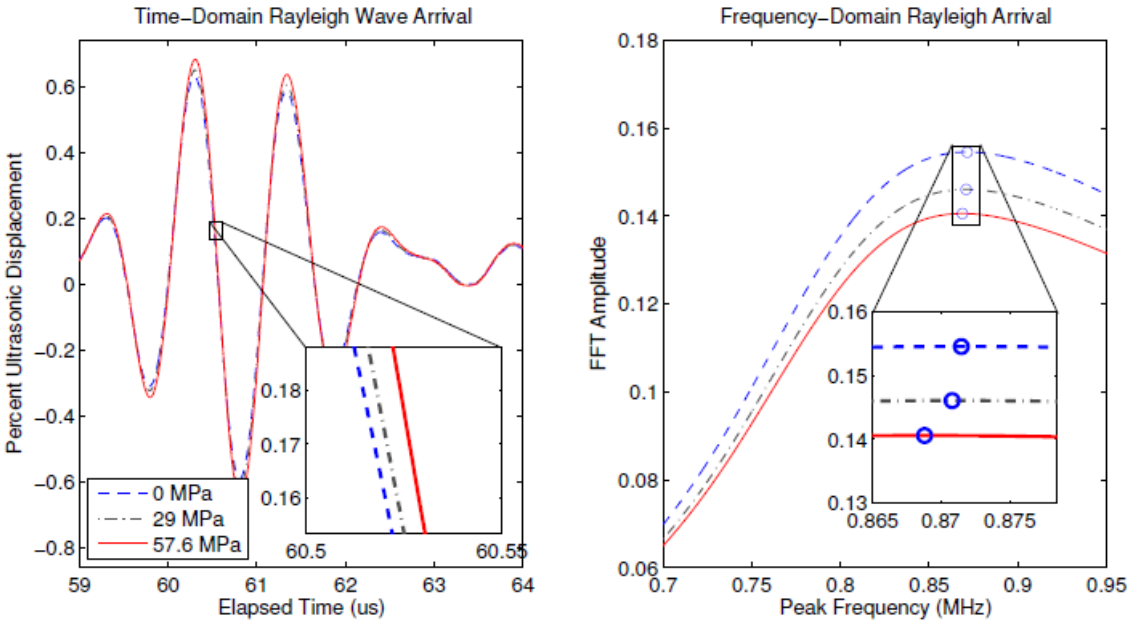

FIGURE 3 Time domain and frequency domain ultrasonic data for three stress states of uniaxial loading test.

The dataset obtained from the constantly coupled measurements generally displays a consistently uniform response over the tensile and compressive stress regions. The largest deviation from the linear slope occurs during the lowest loading steps. The change in frequency per stress is about 28 Hz/MPa, which requires extremely careful testing to consider all the uncertainties in measurement including coupling, surface texture, and equipment.

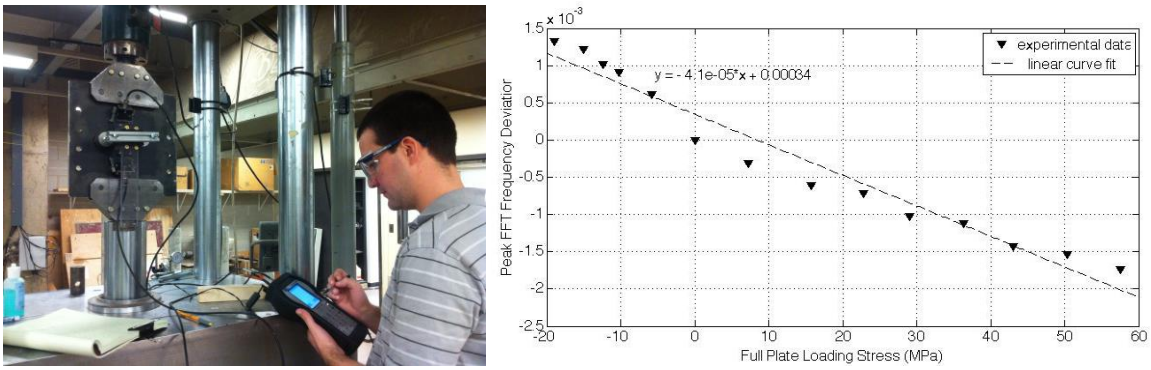

FIGURE 4 (a) Constantly coupled uni-axial tests, (b) stress peak frequency relationship.

(2) Biaxial test – no shear stress

The biaxial test is performed on a 0.375 in. (9.2mm) painted plate. The sensor handle was placed parallel with the direction of the vertical applied loads. The method of loading started with zero load, then set a horizontal load of 5 kN and step increased the vertical loading from 0 - 20 kN. Waveforms were saved at each load step. The horizontal loading was then increased to 10 kN and the vertical loading was step increased again. The change in the peak frequency with stress is plotted in FIGURE 5. The vertical load (parallel to sensor) and horizontal load (perpendicular to sensor) directions will be defined as directions 1 and 2 respectively. For this loading scheme, K_2 from equation 5 can be defined by the average slope between equivalent vertical stress stages at different horizontal stages, which resulted in an average of 4.01×10^{-4} MPa^{-1} as K_2 coefficient. Using Equation 2, the effect of horizontal stress can be removed from the original frequency measurement to quantify K_1. FIGURE 5b presents the adjusted frequency leaving a slope of K_1 as -4.25×10^{-5} MPa^{-1}, which is close to the uniaxial coefficient. The time window for calculating the peak frequencies 59.98 μs to 62.98 μs (corresponds to 300 points of data from the arrival of Rayleigh wave), slightly different than uniaxial test due to minor changes in the experimental setup, which were not fully controllable (e.g., wedge angle). It is recognized that the selection of time window plays a critical role in extracting peak frequency information. If the window is larger, the influences of other waves cause incorrect measurement; if the window is smaller than two cycles, there are insufficient data points to calculate the peak frequency.

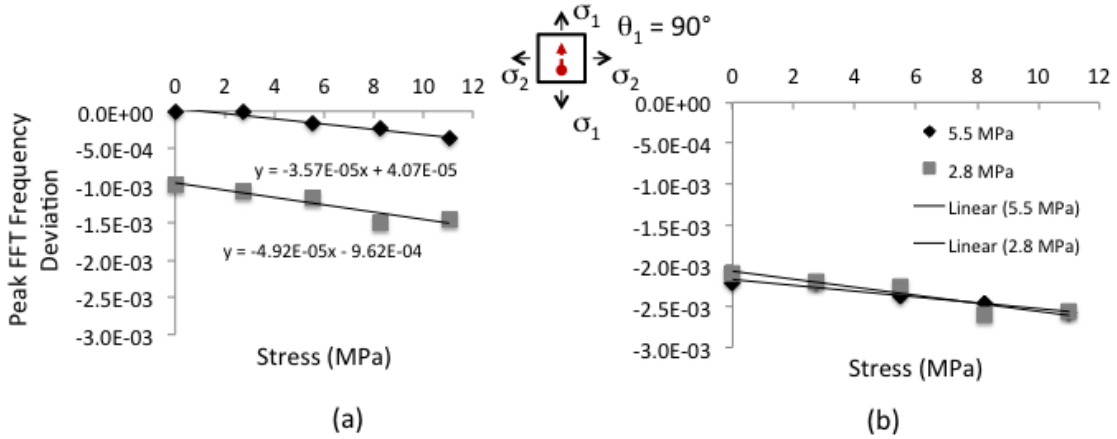

FIGURE 5 Stress vs frequency change when no shear stress exists; (a) uncorrected data, (b) corrected data with K_2.

(3) Biaxial test – the presence of shear stress

The third case includes the measurement device oriented at 42° with respect to vertical line so that shear stress was present in parallel to the sensors line, FIGURE 6a. The angled horizontal and vertical normal stresses were identified according to the sensors orientation. FIGURE 6b shows the results for two different horizontal stress values. Unlike the previous parallel biaxial test, two separate increasing horizontal load steps do not align to a uniform single linear dataset along the parallel component of stress with the perpendicular component removed. This lack of conformity points to a possible additional term missing from equation 6 due to the presence of shear stress. The observed shear behavior may be

due to deeper surface penetration of the perturbation frequency. The deeper surface penetration of the surface wave is desirable due to reducing the effect of paint or surface conditions.

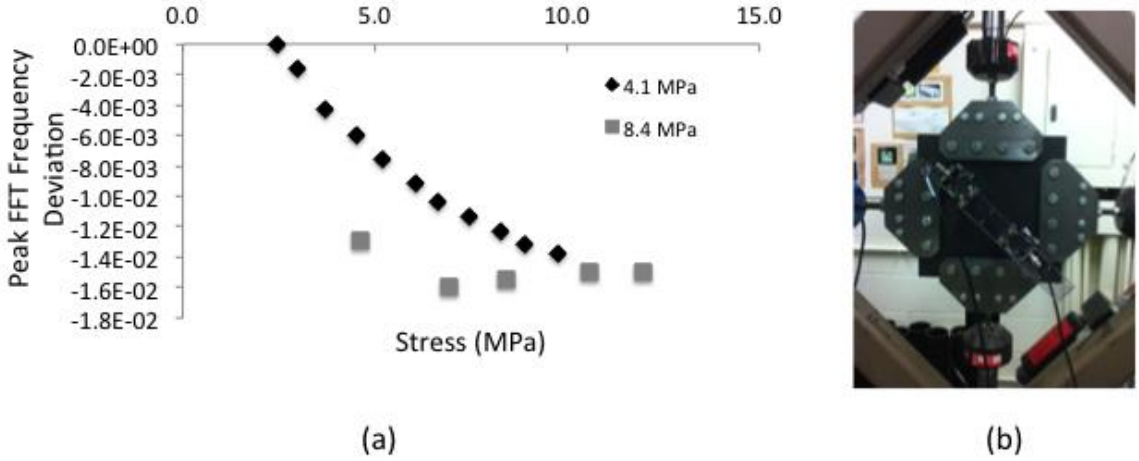

FIGURE 6 Stress versus frequency change when shear stress exists; (a) uncorrected data, (b) a photograph of biaxial experimental setup with the angled measurement.

IMPLEMENTATION CHALLENGES

(1) The Influence of Paint

Steel members usually have a protective layer on the surface, which may not be uniform due to time dependent deterioration. The experimental studies show the dependence of stress-free frequency to the presence and thickness of paint. Steel truss bridges are coated with a standard corrosion protective zinc based primer followed by a urethane top coating. To determine the magnitude of the paint effect a 0.375 in. (9.2 mm) sample was painted following the Illinois Department of Transportation Bridge Paint Specification (GBSP 25). A test was performed recoupling the handheld wedge and measuring the peak frequency and deviation for a group of 10 recouplings at each stage. Three stages of paint conditioning were evaluated as captured in FIGURE 7. The first stage was an unpainted hot-rolled sample. The second stage was a fully painted sample. The third stage was a painted sample with the wedge coupling area ground clean with a wire brush. FIGURE 8 presents the results of the tests.

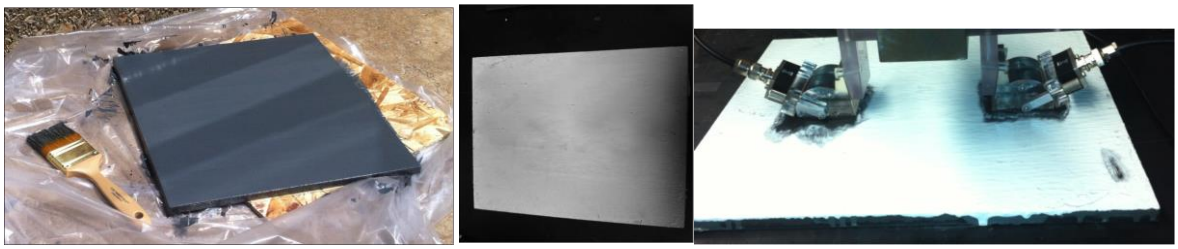

(a) (b) (c)

FIGURE 7 Laboratory brush painted protective zinc based coating; (a) grey zinc primer applied, 1st coat, (b) white fast clad urethane applied, 2nd coat, (c) wire brushed paint sample.

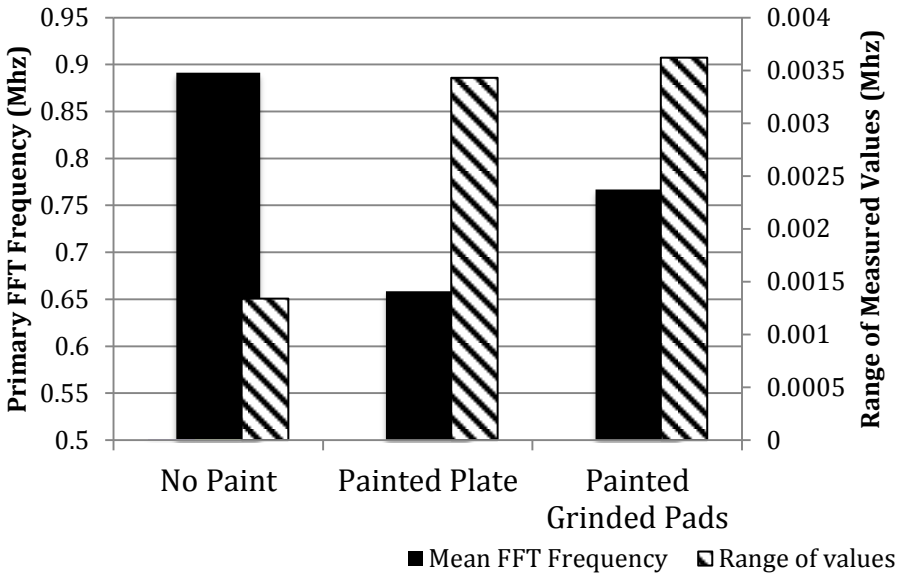

FIGURE 8 The influence of paint on the ultrasonic frequency.

The peak frequency for the painted sample is 0.66 MHz while the unpainted sample is 0.89 MHz. This distinct shift was accompanied by an increase in standard deviation. The grinded coupling area measured a peak frequency of 0.76 MHz, but no decrease in experienced deviation. The results of the paint trial confirm the hypothesis that the painted condition plays an important role on the properties of repeatability in peak frequency identification. Method of stress identification will need to compensate for the unique paint effect of each steel installation. The painted surface recoupling test highlights the need to generate an understanding of the painted sample difference in frequency shift due to stress. Liu et al. [30] showed that the coating thickness influences the Rayleigh wave arrival; however, the change in time of flight with stress is not influenced significantly up to 150 MPa stress. Therefore, the challenge of reference frequency for stress-free surface is addressed in this study through using localized regions of low stress on the gusset plate to generate a baseline measurement to compare against other expected high stress regions.

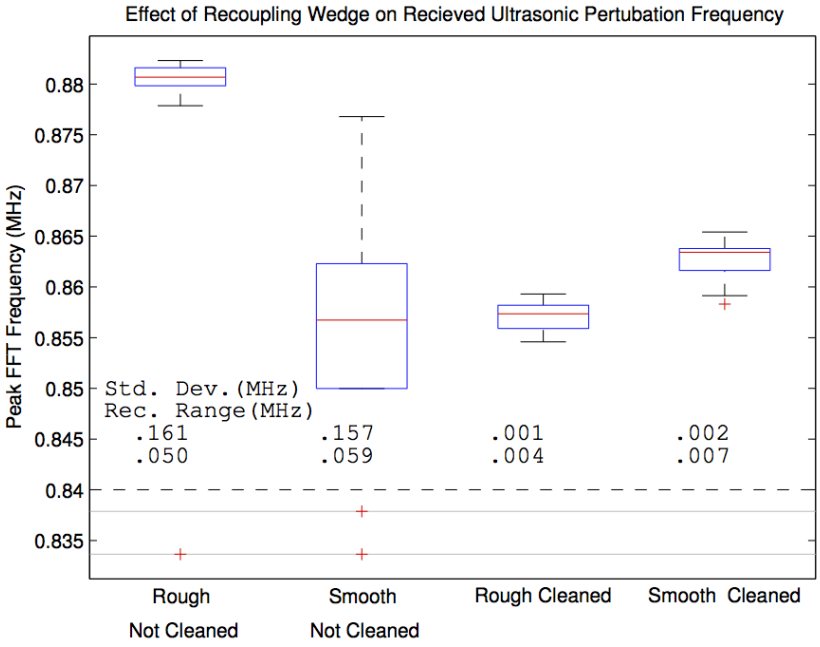

FIGURE 9 The influences of surface roughness and recoupling on the ultrasonic frequency.

(2) The Influence of Recoupling Error

Contact coupling condition can significantly affect the waveform signature, and its properties such as frequency content and amplitude. The thickness, viscosity and chemical properties of the coupling method all affect the properties of the waveform that is transmitted and received in the media. To measure the effect of coupling fluid, two distinct methods were localized and performed with repeatability. The first method was to apply a dime diameter of coupling fluid on the wedge, then attach and remove without wiping excess coupling fluid (Not Cleaned). The second method was to wipe the excess coupling fluid off (Cleaned) in-between attaching the sensor wedges. The results were also performed for both a hot-rolled (Rough) sample and a machine-ground (Smooth) sample. The addition of this blocked variable was to observe potential surface influence and provide an additional data set for the coupling effect. The results of 10 coupling repetitions are presented in FIGURE 9 as a box plot with compressed outliers for the Not Cleaned sample sets. The Not Cleaned samples of Rough and Smooth surfaces have a standard deviation of 0.161 MHz and 0.157 MHz, respectively. While the Cleaned samples have a standard deviation of 0.001 MHz and 0.002 MHz. This provides a reduction factor of 100 in range of recorded peak perturbation frequency. Some potential causes may be that the excess couplant dampens the surface or by wiping the surface to remove excess couplant a relatively smoother surface results. A roughness effect on wave arrival time is reported by Hu et al. [31] based on the residual error of wave velocity measurements. The resolution and errors in this test did not provide consistent results to confirm the findings.

As discussed above, the peak frequency was observed to be critically sensitive to coupling characteristics. To alleviate the sensitivity due to the couplant-effect Sun et al. [28] devised a testing method to isolate the effect of each individual wedge on the target measurand. The method created transmitted a tone at one frequency f_1 and measured the resulting amplitude at the harmonics. Next a second tone at a measured harmonic f_2 was introduced, followed by a response from the receiving transducer at f_1. The ratios of the amplitudes and frequencies allowed the couplant-effect to be identified and decreased from the desired measurand. The experimental results were successful at obtaining decreased deviation in the second harmonic non-linearity measurements. Unfortunately during initial tests implementing the method requires the use of the first order harmonics of a tone-burst waveform instead of the planned spike waveform. Upon the implementation of the tone-burst waveform, the acoustoelastic stress effect was observed to decrease. In order to adapt the method of adjusting the measurand according to unique coupling characteristics of each transducer wedge a new modified non-harmonic method was needed.

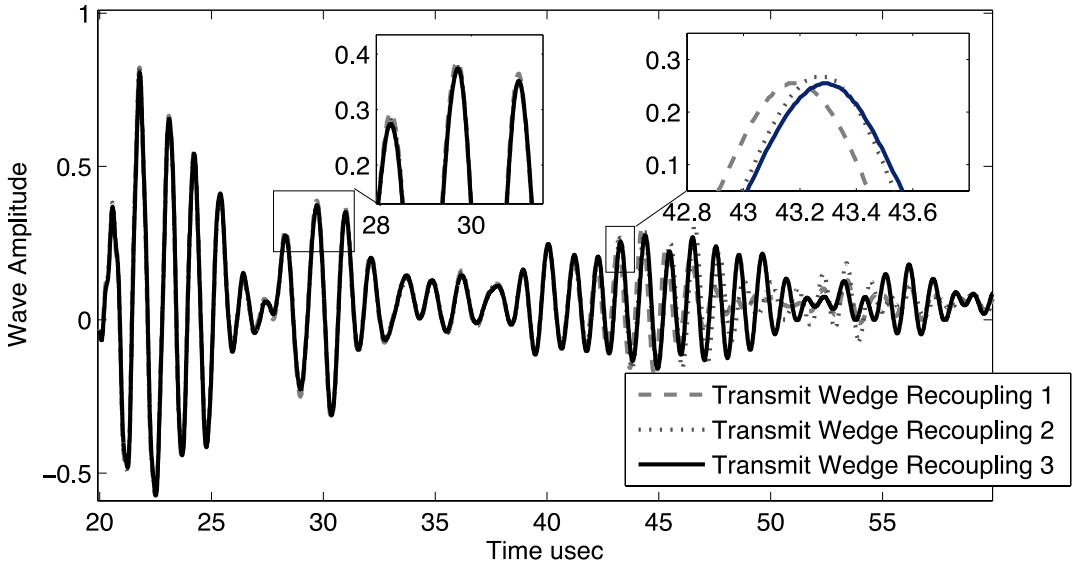

FIGURE 10 Time domain pulse-echo coupling shift.

It was identified that generating a pulse-echo measurement for each wedge, a waveform region near 40 μs distorted upon each recoupling as shown in FIGURE 10. The windowed fast Fourier transform peak frequency on the uncoupled wedges was used as a reference baseline measurement. After each subsequent recoupling, a pulse-echo measurement was generated for each wedge and differenced against the baseline measurement. The change in peak frequency of each wedge as recoupling occurred was visually correlated with the observed error in the through transit peak frequency measurement. The two new sets of pulse-echo frequency were applied as a linear filter to the through transit peak

frequency measurements. The concept of this effect is presented in Equation 5. Through the use of symmetry or constant loading of the material keeping *P* constant, the coupling effect was reduced. From values obtained for the coupling effect, the remaining measured variable was the material stress response (*P*).

$$F_n = I(f)C_{T_n}(f)P(f)C_{R_n(f)}O(f) \tag{5}$$

where F_n is the measured through transit peak frequency for recoupling instance *n*, *I(f)* is input characteristics of transmitter, $C_{T_n}(f)$ and $C_{R_n}(f)$ are the wedge coupling effects (transmitter and receiver wedges) for recoupling instance *n*, *P(f)* is the material stress response, *O(f)* is output characteristics of receiver. Equation 6 provides the proposed experimental implementation of the theoretical Equation 5.

$$F_n - c_1\left[\frac{F_{T_n}-F_{T_c}}{F_{T_c}}\right] - c_2\left[\frac{F_{R_n}-F_{R_c}}{F_{R_e}}\right] = P_n \tag{6}$$

where F_{T_c} is the baseline uncoupled measured peak frequency of the transmitting wedge, F_{T_n} is the measured peak frequency of transmitting wedge for recoupling *n*, F_{R_c} is the baseline uncoupled measured peak frequency of the receiving wedge, F_{R_n} is the measured peak frequency of receiving wedge for recoupling *n*, c_1 and c_2 are contribution factors. F_{T_n} and F_{R_n} are obtained from the pulse-echo mode of transmitter and receiver, respectively.

The pulse-echo method of measurement for each wedge was performed for a series of seven repetitions. Since the contribution of frequency deviation in each wedge was only a percentage of the total error experienced in the through transmission, a factor of contribution is needed. To determine the optimum contribution factor at least two identically stressed regions need to be measured to match the material responses (P_n) term of Equation 6. With the two or more sets of Equation 6 the contribution factors (c_1, c_2) are solved for by minimizing the total remaining error among the P_n solutions using Excel solver tool. With the best-fit contribution factors, the effect of coupling is reduced from all of the through transmission measurements and the resulting shift due to the material response (P_n) is identified. The measured frequencies without any signal processing are plotted in FIGURE 11a. The original transmission and the corrected response shift for each wedge's pulse-echo measurement is presented in FIGURE 11b. From the results in FIGURE 11a, the percent frequency shift in the through transit frequency is inverse of the percent frequency shift in the transmit wedge pulse-echo. Through the proper optimization factors the percentages cancel out to decrease the overall deviation of the measurement. The results presented in FIGURE 11b show a strong decrease in variation towards a consistent measured frequency response for the single stress state. The first measurement in the series experiences the largest error; it is suggestive that this measurement represents the additional human error of initial setup/connections of the system. After applying the optimized factors for both additional pulse-echo measurements the overall frequency deviation is reduced by 35%.

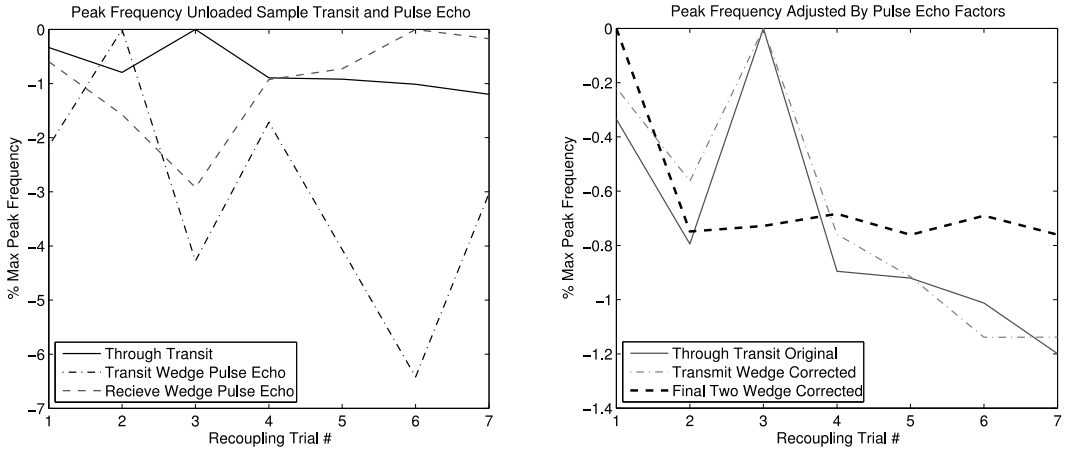

FIGURE 11 Stress-free ultrasonic frequency change per repeated coupling, (a) before correction, (b) after correction.

FIELD DEMONSTRATION

(1) Illinois, Chicago

The fracture critical truss bridge selected was a Pratt Truss bridge. The bridge was originally constructed in 1931 with a total truss span of 227.5 ft (69.3 m) and a width of 56 ft (17.1 m). The bridge spans the Calumet River allowing Halsted Street to with four lanes of traffic. The bridge is located at approximately south 131st street. The foundation of the truss is provided by a concrete column based at the water edge spanning the width. The region of interest for the Illinois Department of Transportation is the gusset plate (L10) directly above the columns. Access to the bottom side of the truss was provided by an inspection trolley directly underneath the lowest chord. The trolley access was critical in obtaining the ability to reach the gusset plate.

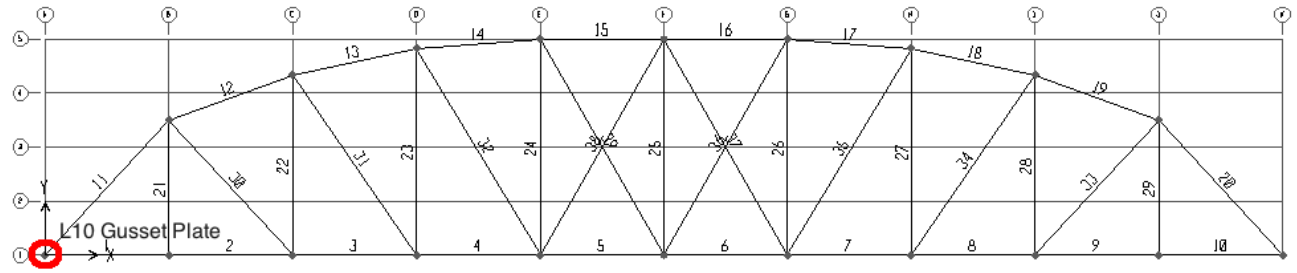

FIGURE 12 SAP2000 bridge overview.

Initially, a finite element model was constructed in SAP2000 to observe the entire structural loading of the bridge. The SAP2000 model was constructed by generating the weight and properties of each build-up shape. Next the resulting loads from the full structure were integrated into a finite element model of the target gusset plate. The dead loads carried by each truss element connected to the gusset plate are provided in the drawing. The loads used for this project are based upon the bill of materials within the set of historical drawings. First, the longitudinal members were constructed and a weight generated. Then based on the general structural drawings the remaining total weight was distributed evenly over the structure. Special attention was paid to the rivet locations and numerical counts to best match the field conditions. The generated drawing of the gusset plate was imported into the COMSOL modeling environment. Methods for numerical model construction were based upon relevant developing publications (Liao et al., 2011). A COMSOL finite element solution was constructed to provide details on the complex loading responses of the gusset plate. To model the proper stress response the boundary conditions were assigned as an axial displacement along the 43^{o} vertical member and a simulated pin connection. The simulated pin connection fixed the center of the bottom left connection and distributed the resulting forces to the relative surrounding rivets. This pair of boundary conditions allowed for plate expansion on all of the member connections. The vertical local deck connection was removed from the model due to the low relative load and to reduce the model complexity.

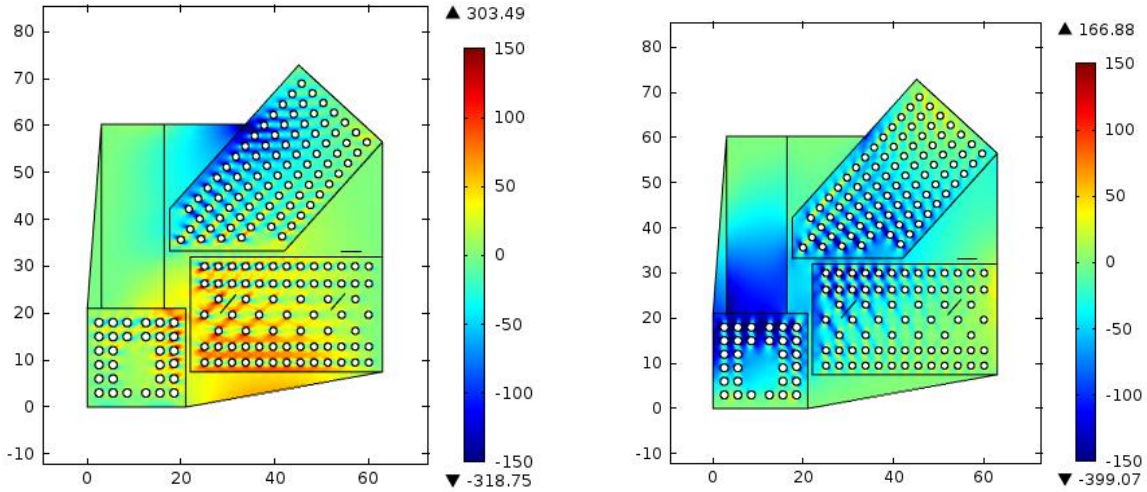

FIGURE 13 Gusset plate numerical model stress solution; a) horizontal normal stress model, b) vertical normal stress model (MPa).

The results of the finite element model are presented in FIGURE 13. The graphical model shows a region of higher magnitude stress extending of the fixed pin at a 45 degree angle through the bottom chord connection towards the angled chord. The region directly around the fixed pin rivets may be artifact of the constrained boundary condition placed on the rivets. The placement of sensor locations was designed to provide one low stress region and one complex high stress region. The finite element model presented confirms that the sensor placement was in a mixture of high stress and low stress regions.

To provide a field measurement the following procedure was followed. Pictures of the gusset plate region are provided in FIGURE 14, with visible identical plates on both sides of the joint. To maximize the benefit of available loading symmetry with a gusset plate on each side of the beam, measurements were taken at the same locations on each side. Also, to minimize possible human error, a magnet mounting bracket was constructed for the wedge holder. The magnet mount was tested in the laboratory and found to have no noticed effect on the piezoelectric transducer responses. Photos of the sensor coupled to the gusset plate are provided in the figure. Once the transducers were coupled, a series of three waveform measurements were performed: pulse-echo transmit wedge, pulse-echo receive wedge and a through transmission. For each waveform measurement three waves were recorded for averaging and confirmation. It is important to note that the traffic load was varying during the measurement. Multiple measurements from a given location minimize the effect of traffic load on the ultrasonic measurement to identify the dead load stress. This process was repeated for both sides of the gusset plate. The three trial critical variables in the through transmission mode are transmitter coupling, stress frequency shift and receiver coupling. Due to symmetry, the stress frequency shift is constant between the two measurements, then the remaining change in waveform frequency is resulting from the coupling condition.

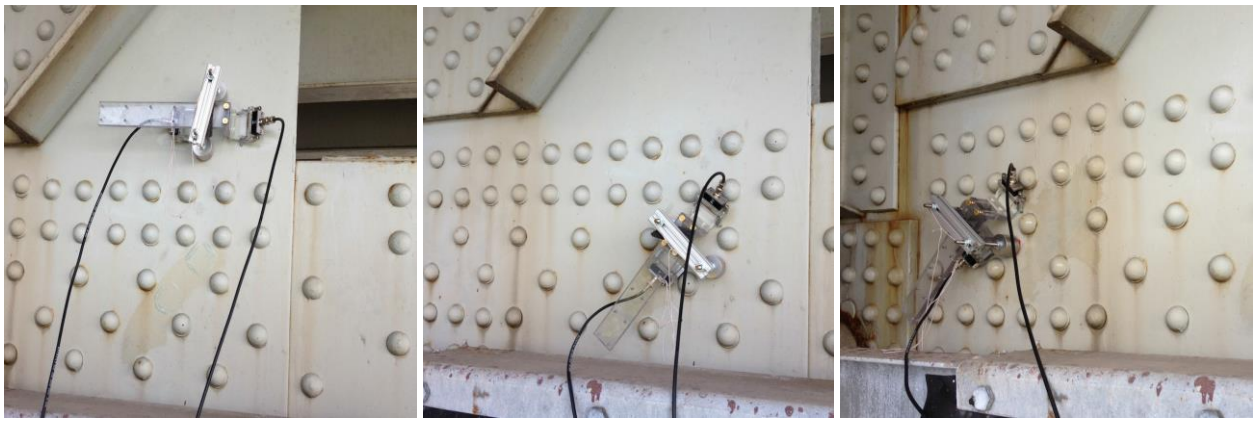

FIGURE 14 Coupled ultrasonic wedge sensor in positions A, B, C respectively.

The peak Rayleigh wave frequencies obtained from six measurement locations using through transmission mode are provided in FIGURE 15a. The pulse-echo approach discussed above to reduce the coupling error is applied to the data and presented in FIGURE 15b. Reducing the coupling error in the field measurement is a critical factor, especially as the ultrasonic frequency shift with stress is relatively weak. In the uncorrected field measurements, FIGURE 15a, no consistent frequency shift per measurement location is obtained. From the corrected measurements, the peak frequencies at the symmetric measurement points are very close to each other. Additionally, the measurement points C1 and C2 are located at the highest stressed points of the gusset plate and the peak frequencies obtained from these points are the lowest, which agrees with the theory.

In testing the bridge in Illinois, measurement only in one direction was taken. However, the laboratory experiments show the relationship between horizontal and vertical stresses in directions of measurement axis, and ultrasonic frequencies. In next field testing in Virginia, measurements were taken in two orthogonal directions, and the resultant stresses were compared with the finite element model.

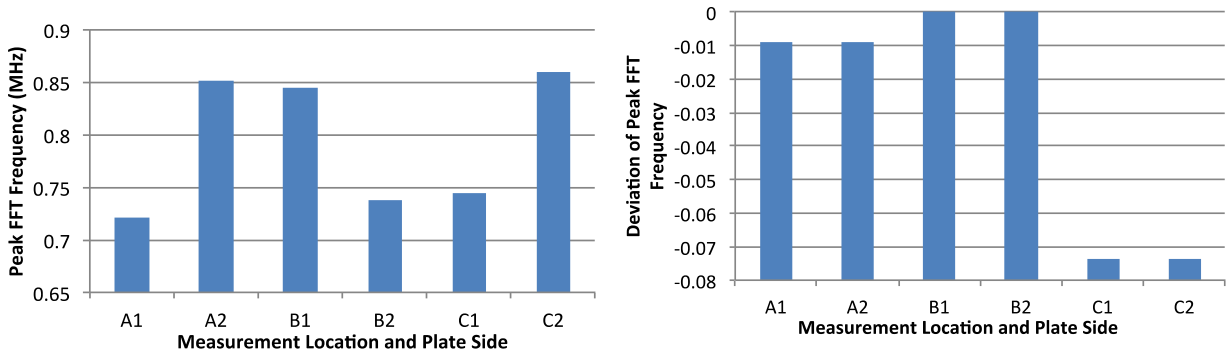

(a) (b)

FIGURE 15 Through transmission results, (a) uncorrected, (b) corrected.

(2) Norris Bridge, Virginia

The second bridge test was conducted on Norris Bridge, Virginia. The Robert O. Norris Jr. Bridge, which carries Route 3, spans the lower Rappahannock River, Virginia. This structure has a total length of about 10,000 feet consisting of forty-four spans of varying construction. The measurement was taken at the through truss main spans as shown in FIGURE 16.

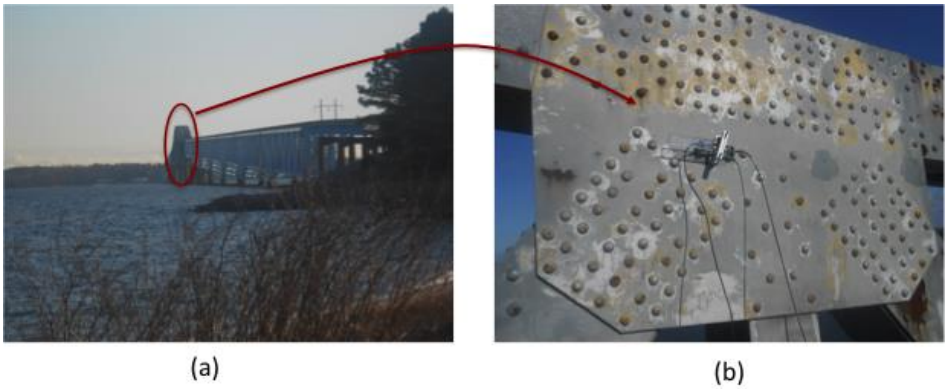

FIGURE 16 Norris Bridge, (a) general view, (b) gusset plate tested in the through truss main span.

A finite element model of the truss bridge was constructed in COMSOL Multi-physics software. When the gusset plate is modeled without full geometry, the model lacks real boundary conditions necessary for an accurate analysis. Therefore, a multi-scale numerical modeling was implemented in order to simulate the gusset plate boundary conditions properly without having the need to model the full scale structure. FIGURE 17 shows the multi-scale modeling approach. In the model the gusset plate was modeled in the full scale details along with half of the beam element connecting it with the remaining truss structure in order to avoid the stress concentration. On the other hand, the overall truss bridge components were modeled as beam elements in order to simplify the overall analysis of the bridge. Within the COMSOL software the two-dimensional space was used, and three different physics were added to the model. The gusset plate was modeled with solid mechanics physics and for the rest of the truss the physics used were beam and truss physics (beam for the most of the elements and truss for the element with hinged joints). In order to make an integrated model the displacement and rotation of the gusset plate and beam elements were combined together. Steel material with default properties in the program was selected. The model was then analyzed statically and the stresses of the x, y and xy directions were extracted. The bridge loads were obtained from the as-built drawings.

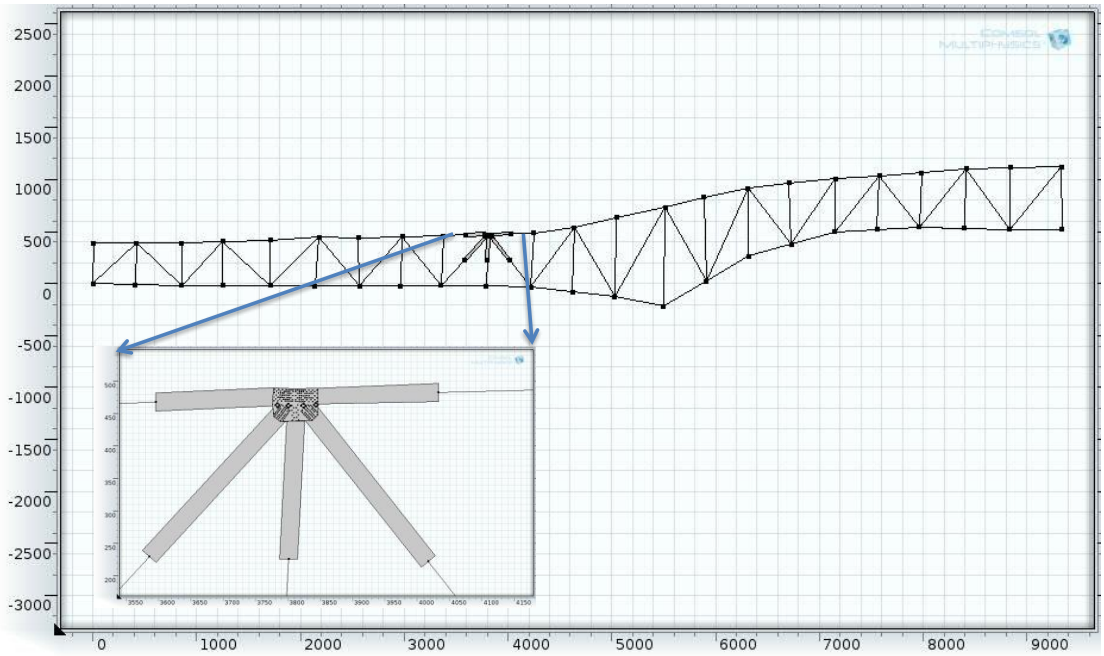

FIGURE 17 Multi-scale bridge model of complete truss elements and plate elements (inset) for modeling gusset plate.

FIGURE 18 shows the normal and shear stress distributions on the gusset plate. The circles shown on the images indicate the places of the ultrasonic measurements. The measurement in locations 1 to 3 were taken both horizontal and vertical directions, and reported in this report.

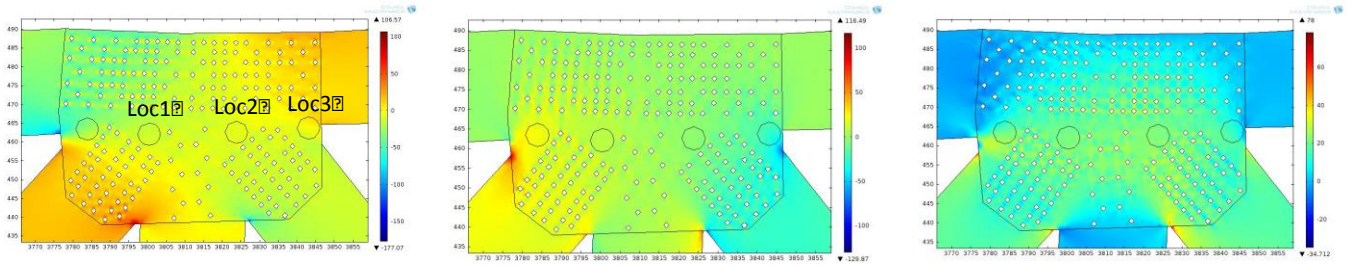

(a) (b) (c)

FIGURE 18 Stress distribution on the gusset plate, (a) stress in x direction σ_{xx}, (b) stress in y direction σ_{yy}, (c) stress in xy direction σ_{xy}.

The stresses obtained through ultrasonic measurement without and with coupling correction methods are shown in FIGURE 19. There are six measurements in each location. The first three measurements are vertical directions, and the ultrasonic transducers were recoupled at each measurement. The last three measurements are repeated tests at horizontal directions. There are significant variations from one recoupled test to another. The correction factors are identified through defining the difference in measurements as zero, and applied in FIGURE 19b. The corrected data has consistent values for a given particular location and direction.

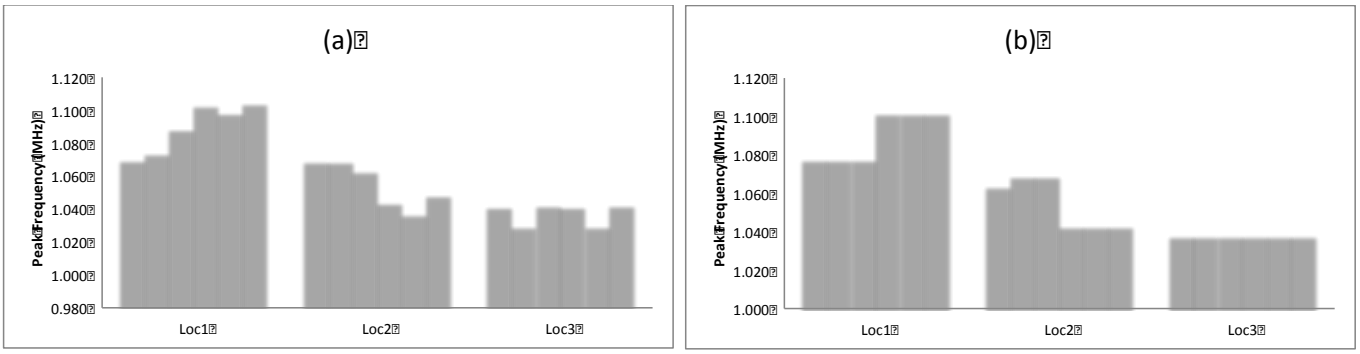

FIGURE 19 The measured peak frequency, (a) before coupling correction, (b) after coupling correction.

Using the corrected peak frequency values, Equations 3 and 4, and nonlinearity coefficients obtained from biaxial loading, the stresses in vertical (y) and horizontal (x) directions are calculated and shown in TABLE 1. While there is significant difference between two methods, the error calculation considering entire elastic stress range as ± 250 MPa results in acceptable values.

TABLE 1 Comparison of experimental and numerical results.

Location		FE Stress (MPa)	Peak Frequencies Repeated Tests (MHz)					Calculated Stress (MPa)	Error %
			Transmitter pulse-echo	Receiver pulse-echo	Through transmission	Adjusted through transmission	Difference to f_o		
1	S_{yy}	8.04	9.81E-01	1.03E+00	1.07E+00	1.08E+00	3.83E-02	164.7	1931.33
			9.85E-01	1.03E+00	1.07E+00	1.08E+00	3.83E-02	164.7	1931.33
			9.87E-01	1.03E+00	1.09E+00	1.08E+00	3.83E-02	164.7	1931.33
	S_{xx}	-13.04	9.08E-01	8.87E-01	1.10E+00	1.10E+00	6.16E-02	112.0	962.00
			9.08E-01	8.87E-01	1.10E+00	1.10E+00	6.15E-02	112.0	962.00
			9.08E-01	8.87E-01	1.10E+00	1.10E+00	6.15E-02	112.0	962.00
2	S_{yy}	-4.23	9.20E-01	1.01E+00	1.07E+00	1.06E+00	2.48E-02	19.5	561.75
			9.20E-01	1.02E+00	1.07E+00	1.07E+00	2.97E-02	19.5	561.75
			9.19E-01	1.02E+00	1.06E+00	1.07E+00	2.97E-02	19.5	561.75
	S_{xx}	-7.83	8.99E-01	9.16E-01	1.04E+00	1.04E+00	4.95E-03	72.0	1019.97
			8.99E-01	9.16E-01	1.04E+00	1.04E+00	4.95E-03	72.0	1019.97
			9.00E-01	9.17E-01	1.05E+00	1.04E+00	4.95E-03	72.0	1019.97
3	S_{yy}	-3.55	1.01E+00	8.03E-01	1.04E+00	1.04E+00	-6.42E-16	0.0	100.71
			1.01E+00	8.02E-01	1.03E+00	1.04E+00	8.56E-16	(0.0)	100.71
			1.01E+00	8.02E-01	1.04E+00	1.04E+00	2.14E-16	(0.0)	100.71
	S_{xx}	-24.66	8.89E-01	9.13E-01	1.04E+00	1.04E+00	4.28E-16	(0.0)	1004.93
			8.91E-01	9.13E-01	1.03E+00	1.04E+00	0.00E+00		1004.93
			8.94E-01	9.12E-01	1.04E+00	1.04E+00	2.78E-15	(0.0)	1004.93

Another factor that is not considered in the calculations is shear stress. As shown in numerical results, there is significant shear stress at the measured locations. For example, shear stress at location 1 is about 22 MPa. Typical Rayleigh wave penetration depth is one wavelength. For instance, the depth of penetration for 1 MHz (selected frequency in this study) is 3 mm while it is 1 mm for 3 MHz frequency. With the hypothesis that if ultrasonic wave is coupled with the fraction of cross section, the change in ultrasonic properties due to shear stress is affected by the depth of penetration. FIGURE 20 indicates the penetration depth of Rayleigh waves, which depends on the selected frequency, and the shear stress distribution at a traction free surface. When the frequency is increased, the penetration depth $t_{Rayleigh}$ becomes smaller; therefore, ultrasonic waves are not influenced by the presence of shear stress. For instance, 5 MHz, Rayleigh waves stay on the surface where shear stress is zero. The correlation between the depth of penetration and shear stress needs to be formed, which is the future work of this study.

FIGURE 20 Rayleigh wave and shear stress distribution per depth.

PLANS FOR IMPLEMENTATION

From these field results multiple issues relating to accuracy and repeatability have been uncovered. The increased shear stress present in the field gusset plate may have an additional role upon the individual acoustoelastic coefficients. The increased loss of accuracy at the lower stress regions of the plate may also be a factor of the additional non-linearity of the stress frequency calibration curves. Also, finite element modeling of in-situ gusset plates is still a developing research topic, error within the model and inputs is another region of inaccuracy.

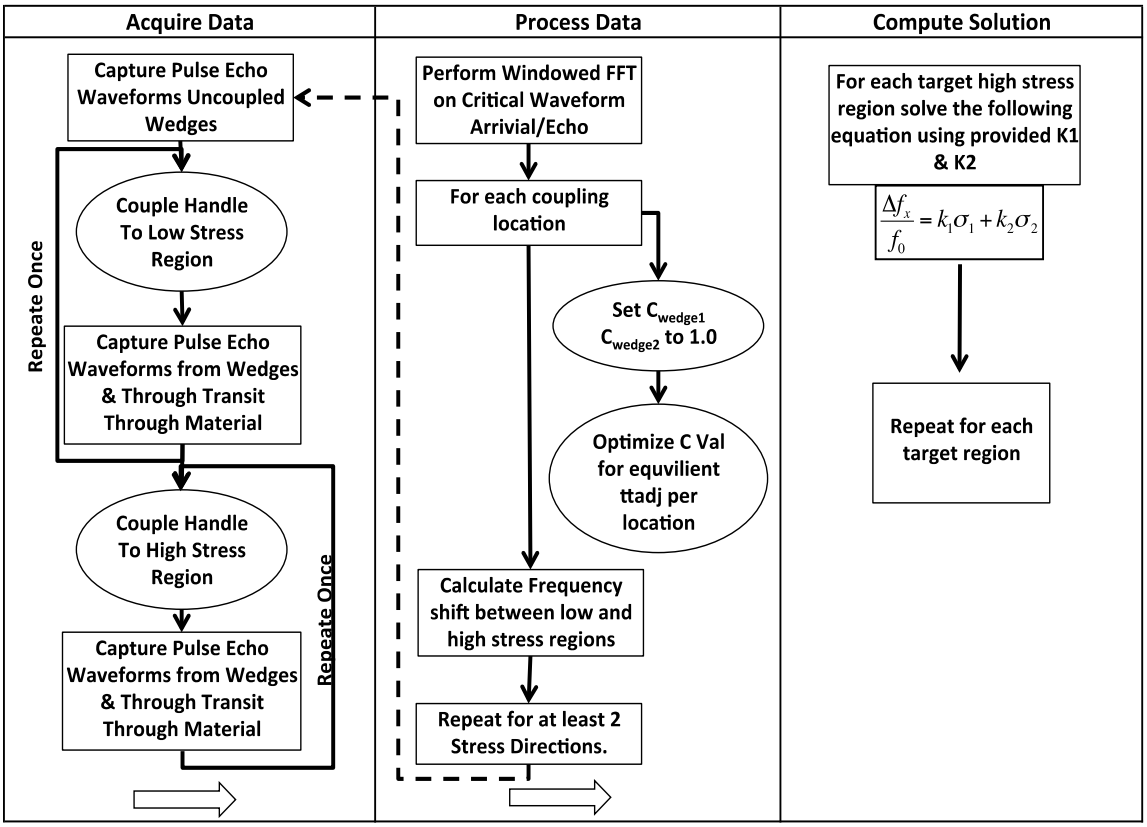

FIGURE 21 The proposed stress measurement methodology for gusset plates.

CONCLUSIONS

Stress identification within existing structures is a critical field for the existing aging infrastructure network. The general purpose behind the project presented in this report is to provide a quantitative window into fracture critical steel gusset plates. The ability to understand existing loads and determine unexpected changes in loading is critical to the long term safety and stability of these structures. Through the acoustoelastic properties of steel the method of ultrasonic stress identification has been applied. The goal was to further the understanding of the acoustoelastic response in the frequency-domain. Prior surface wave stress frequency calibrations could not be found in published literature.

The first task of generating suitable experimental stress frequency calibration curves was taken in multiple steps. With each test increasing knowledge about the behavior of each of the testing parameters developed. The coupling conditions were found to be a critical factor and required developing a method of quantitative adjustment. The pulse-echo method of calibration was constructed to allow adjustment for coupling abnormalities. Used in areas of symmetry or similar loading, this method proved to consistently reduce coupling errors. The remaining factor of paint thickness was addressed by generating multiple pairs of coefficients, one for each paint case. The last factor of thickness was resolved to behave precisely as the numerical model calculated.

With the fundamental uniaxial process captured, the focus of investigation turned to application restrictions. Installed steel gusset plates are not ideal uniaxial structures with free surfaces. Further load testing was performed to determine the biaxial response of the frequency stress correlation. Previously no surface wave acoustoelastic publications have contained simultaneous two-direction loading waveform measurements. The published acoustoelastic stress velocity theory resolved the stress frequency relationship when the loading was applied parallel with the coupled sensor. In pursuit

to model an arbitrary angle as experienced in the field, the acoustoelastic stress velocity theory failed to provide a satisfactory explanation for the entire frequency shift experienced.

Progressing beyond the laboratory, two field tests were procured and measurements were per-formed upon two truss bridges. Numerical models were constructed of the bridges along with a focused model of the gusset plate. Based on the field conditions, two additional factors effecting measurement, paint thickness and constant coupling were identified and mitigated. For a uniform coupling over the course of multiple waveform readings a magnetic holder was constructed. Applying the results measured on the plate with the numerical model, the concept of measuring a frequency to determine stress state appears valid. The error compared to the numerical model was found to be a successful result for the first initial field based direct application. Further refinement of the complex stress correlation will be needed in order to quantify the expected error obtained through this means of measurement.

REFERENCES

1. Liao, M., Okazaki, T., Ballarini, R., Schultz, A. and Galambos, T. (2011). "Nonlinear Finite-Element Analysis of Critical Gusset Plates in the I-35W Bridge in Minnesota," Journal of Structural Engineering, Vol. 137, pp. 59–68.

2. Hughes, T.G. and Pritchard, R. (1998). "In Situ Measurement of Dead and Live Load Stresses in a Masonry Arch," Engineering Structures, Vol. 20, No. 1-2, pp. 5-13.

3. Wardhana K., and Hadipriono F.C. (2003). "Analysis of Recent Bridge Failures in the United States," Journal of Performance of Constructed Facilities, Vol. 17, pp. 144–150.

4. Hughes D.S., and Kelly J.L. (1953). "Second Order Elastic Deformation of Solids," Physical Review, Vol. 92, No. 5, pp. 1145-1149.

5. Gerhart, G.R. (1976). "Rayleigh Wave Velocity for a Stress-induced Slightly Anisotropic Solid," Journal of the Acoustical Society of America, Vol. 60, No. 5, pp. 1085-1088.

6. Junge M., Jacobs L.J., Qu J., Jarzynski, J. and La Saponara, V. (2004). "The Measurement of Applied Stress using the Polarization of Rayleigh Surface Waves," Review of Quantitative Nondestructive Evaluation, Vol. 23, pp.1187–1192.

7. Heyman, J.S. and Chern, E.J. (1982). "Ultrasonic Measurement of Axial Stress," Journal of Testing and Evaluation, Vol. 10, No. 5, pp. 202-211.

8. Chen, H.L. and Wissawapaisal, K. (2001). "Measurement of Tensile Forces in a Seven-wire Prestressing Strand using Stress Waves," Journal of Engineering Mechanics, Vol. 127, pp. 599-606.

9. Rizzo P., and Lanza di Scalea F. (2003). "Effect of Frequency on the Acoustoelastic Response of Steel Bars," Experimental Techniques, Vol. 27, Issue 6, pp. 40–43.

10. Chaki S., and Bourse G. (2009). "Stress Level Measurement in Prestressed Steel Strands Using Acoustoelastic Effect," Ultrasonics, Vol. 49, pp. 673–681.

11. Clark, A.V., Hehman, C.S., Gallagher, D., Lozev, M.G. and Fuchs, P.A. (1999). "Ultrasonic Measurement of Stress in Pin and Hanger Connections," Journal of Nondestructive Evaluation, Vol. 18, No. 3, pp. 103-113.

12. Song, F., Huang, G.L., Kim, J.H., and Haran, S. (2008). "On the Study of Surface Wave Propagation in Concrete Structures using a Piezoelectric Actuator/sensor System," Smart Materials and Structures, Vol. 17, No. 5, pp. 055024.

13. Lillamand I., Chaix J.F., Ploix M.A., and Garnier V. (2010). "Acoustoelastic Effect in Concrete Material under Uniaxial Compressive Loading," NDT & E International, Vol. 43, pp. 655–660.

14. Jassby, K., and Saltoun, D. (1981). "Use of Ultrasonic Rayleigh Waves for the Measurement of Applied Biaxial Surface Stresses in Aluminum 2024-T351 Alloy," Materials Evaluation, Vol. 40, No. 1, pp. 198-205.

15. Hussaon, D., Bennett, S.D., and Kino, G.S. (1982). "Measurement of Surface Stresses using Rayleigh Waves," Ultrasonics Symposium, pp. 889-892.

16. Gandhi, N., Michaels, J.E., and Lee, S.J. (2012). "Acoustoelastic Lamb Wave Propagation in Biaxially Stressed Plates," Journal of the Acoustical Society of America, Vol. 132, No. 2, pp. 1284-1293.

17. Shi, F., Michaels, J.E., and Lee, S.J. (2013). "In Situ Estimation of Applied Biaxial Loads with Lamb Waves," Journal of the Acoustical Society of America, Vol. 133, No. 2, pp. 677-687.

18. Hario M., Fukuoka H. and Hori, K. (1981). "Acoustoelastic Effect of Rayleigh Surface Wave in Isotropic Material," Journal of Applied Mechanics, Vol. 48, pp. 119–124.

19. Arora, A. and James, M.R. (1982). "Ultrasonic Measurement of Residual Stress in Textured Materials," Journal of Testing and Evaluation, Vol. 10, No. 5, pp. 212-216.

20. Sayers, C.M., Allen, D.R., Haines, G.E., and Proudfoot, G.G. (1986). "Texture and Stress Determination in Metals by using Ultrasonic Rayleigh Waves and Neutron Diffraction," Phil. Trans. R. Soc. Lon. A, Vol. 320, pp. 187-200.

21. Zeiger, A. and Jassby, K. (1982). "Measurement of Acoustoelastic Coefficients of Rayleigh Waves in Steel Alloys," Journal of Nondestructive Evaluation, Vol. 3, No. 2, pp. 115-124.

22. Daami, T., Touratier, M. and Castex, L. (1987). "Effect of Plastic Deformation on the Acoustoelastic Response of Some Materials," Experimental Mechanics, Vol. 27, No. 4, pp. 333-337.

23. Berruti, T. and Gola, M.M. (1996). "Acoustoelastic Determination of Stresses in Steel using Rayleigh Ultrasonic Waves," Materials Science Forum, Vols, 210-213, pp. 171-178.

24. Norris A. (1998). Finite-Amplitude Waves in Solids Nonlinear Acoustics.

25. Dos Santos A., and Bray D.E. (2002). "Comparison of Acoustoelastic Methods to Evaluate Stresses in Steel Plates and Bars," Journal of Pressure Vessel Technology, Vol. 124, pp. 354-358.

26. Egle, D.M., and Bray, D.E. (1976). "Measurement of Acoustoelastic and Third-order Elastic Constants for Rail Steel," Journal of the Acoustical Society of America, Vol. 60, No 3, pp. 741-744.

27. Hu X., and Shenton, H.W. (2007). "Dead Load Based Damage Identification Method for Long-term Structural Health Monitoring," Journal of Intelligent Material Systems and Structures Vol. 18, pp. 923–938.

28. Sun, L, Kulkarni, SS, Achenbach, JD, and Krishnaswamy, S. (2006). "Technique to Minimize Couplant-effect in Acoustic Nonlinearity Measurements," Journal of the Acoustical Society of America, Vol. 120, pp. 2500–2505.

29. Thurston, R.N., and Brugger, K. (1964). "Third-order Elastic Constants and the Velocity of Small Amplitude Elastic Waves in Homogeneously Stressed Media," Physical Review, Vol. 133, No. 6A, pp. 1604-1610.

30. Liu, B., Dong, S., Xu, B. and He, P. (2012). "Coating Thickness Affects Surface Stress Measurement of Brush Electro-plating Nickel Coating using Rayleigh Wave Approach," Ultrasonics, Vol. 52, No. 7, pp. 861-866.

31. Hu, E., He, Y., and Chen, Y. (2009). "Experimental Study on the Surface Stress Measurement with Rayleigh Wave Detection Technique," Applied Acoustics, Vol. 70, pp. 356-360.